EES Batteries

PAPER

View Article Online
View Journal

Cite this: DOI: 10.1039/d6eb00040a

Chemo-mechanical deformations in lithium titanate composite electrodes upon over-lithiation

Batuhan Bal,*[a] Bertan Özdoğru,*[a] Marcos Lucero,[b] Bhuvaneswari M. Sivakumar,[b] Vijayakumar Murugesan,[c,d] Xiaolin Li[b] and Ömer Özgür Çapraz*[a,e]

Lithium titanate ($Li[Li_{1/3}Ti_{5/3}]O_4$, LTO) electrodes have received significant attention as anodes for Li-ion batteries due to their "zero-strain" feature, associated with their negligible volumetric changes to form $Li_2[Li_{1/3}Ti_{5/3}]O_4$ during cycling. However, there is not much known about chemo-mechanical instabilities in the LTO electrode when it is over-lithiated to $Li_{2+x}[Li_{1/3}Ti_{5/3}]O_4$ at lower voltages (<1.0 V *vs.* Li). Here, chemo-mechanical deformations in the LTO composite electrode were investigated by conducting *operando* strain and stress measurements in various voltage windows, supported by *ex situ* XPS. The LTO experienced a reversible deformation with a negligible amount of strain when cycled between the 1.0 and 3.0 V voltage window. When polarized to 0.35 V *vs.* Li, the LTO electrode experienced large strains (0.8%) and compressive stress generation, with a significant amount of irreversible deformation. The Li-intercalation-induced strains were predicted using a mathematical model. The predicted strains match well with the strain generation at higher voltages (1.0–3.0 V); however, there is a large misalignment between predicted strains and experimentally measured strains at lower voltages. XPS measurements exhibited the formation of thick SEI layers on the LTO electrodes when cycled at lower voltages. The combination of experimental and predicted strains indicates large deformations between 0.5 and 0.8 V during lithiation, and it was attributed to the formation of SEI layers. Our study provides a comprehensive analysis of the chemo-mechanical deformations in the LTO electrodes in over-lithiated states, and we foresee that a similar approach can be utilized to understand the deformation mechanisms in other zero-strain electrodes in higher states of (dis)charge.

Received 18th February 2026,
Accepted 18th March 2026

DOI: 10.1039/d6eb00040a

rsc.li/EESBatteries

Broader context

Zero-strain electrodes present an opportunity to mitigate instabilities for improved electrochemical performance in alkali metal-ion batteries (*e.g.*, Li-ion and Na-ion batteries). Despite extensive investigations of over-lithiated lithium titanate (LTO) electrodes, there are conflicting reports about the chemo-mechanical deformations in the LTO electrodes when over-lithiated. In this study, we utilized *operando* digital image correlation and a multi-beam optical stress sensor, supported by *ex situ* XPS, to probe *operando* electrochemical strain and stress generation in the LTO electrodes in various electrochemical windows. When cycled between 1.0 and 3.0 V voltage windows, the LTO electrode experiences almost negligible mechanical deformations during cycling. When cycled between 0.35 and 3.0 V, the LTO electrode undergoes severe mechanical deformation. Plastic deformation is attributed to the formation of SEI layers (supported by *ex situ* XPS analysis) and elastic deformation is attributed to the phase changes in the electrode (supported by previous XRD studies). The combination of experimental and predicted strains indicates large deformations between 0.5 and 0.8 V during lithiation, and it was attributed to the formation of SEI layers. Our study provides a comprehensive analysis of the chemo-mechanical deformations in the LTO electrodes in over-lithiated states, and we foresee that a similar approach can be utilized to understand the deformation mechanisms in other zero-strain electrodes in higher states of (dis)charge.

Introduction

The electrochemical performance of battery electrodes strongly correlates with their ability to withstand mechanical deformations over cycling. Particle fracture,[1] generation of isolated particles,[2] and further instabilities in solid-electrolyte interphase/cathode-electrolyte interphase (SEI/CEI) layers[3,4] lead to capacity fading in the battery electrodes. During each charge/discharge process, the intercalation of the metal ions into the

[a]*The School of Chemical Engineering, Oklahoma State University, Stillwater, OK 74078, USA. E-mail: capraz@umbc.edu*
[b]*Pacific Northwest National Laboratory, Richland, Washington 99352, USA*
[c]*Physical and Computational Sciences Directorate, Pacific Northwest National Laboratory, Richland, Washington 99352, USA*
[d]*Joint Center for Energy Storage Research (JCESR), Lemont, Illinois 60439, USA*
[e]*The Department of Chemical, Biochemical, and Environmental Engineering, University of Maryland, Baltimore County, Baltimore, MD 21250, USA*

electrode structure leads to volumetric changes and associated structural stress generation in its structure.[5] Repeated ion intercalation over cycling leads to fatigue in the electrode, eventually leading to particle fracture. These cracks could generate isolated fractured particles in the composite electrode outside of the conductive network.[2] Furthermore, particle fracture leads to an increase in the surface area between the electrode and electrolyte; therefore, the electrode becomes more vulnerable to interfacial instabilities associated with the formation of solid-electrolyte interphase (SEI) layers on anodes or cathode-electrolyte interphase (CEI) layers on cathodes. Continuous volumetric changes in the electrode particles during cycling stretch SEI/CEI layers, and if these layers are not elastic enough, they can lead to plastic deformations and ruptures in these surface layers.[6]

In this aspect, zero-strain electrodes present an opportunity to mitigate instabilities for improved electrochemical performance. A "zero-strain electrode" can be described as an electrode experiencing a negligible amount of volumetric changes in its lattice during metal-ion intercalation (*ca.* <0.2% in the lattice). There have been tremendous efforts devoted to developing zero-strain electrode materials for battery applications to enhance cycling stability.[7,8] Prominent examples of zero-strain electrodes include spinel lithium titanate ($Li[Li_{1/3}Ti_{5/3}]O_4$, LTO),[9,10] sodium vanadium phosphate ($Na_3V_2(PO_4)_3$),[11] potassium nickel hexacyanoferrate (KNHCF),[12–14] layered Li-doped $Na_{2/3}TiO_2$,[15] and spinel $LiCo_{1-x}Al_xO_2$.[16] However, there are conflicting reports in the literature about the facts of the zero-strain electrodes. For example, KNHCF cathodes were claimed to be a "zero-strain" cathode for K-ion batteries based on the previous X-ray diffraction studies.[12–14] *Operando* strain measurements reported about 0.5% reversible strain generation in the composite KNHCF cathode during K-ion intercalation.[17] Understanding the deformation mechanism in the electrodes is critical to developing "zero-strain electrodes".

Among the existing library of zero-strain electrodes, LTO emerges as a compelling candidate for anodes in lithium-ion batteries, particularly due to its zero-strain characteristics, well-defined voltage plateau at around 1.5 V, and fast-charging capability.[18,19] The distinctive feature of LTO lies in its spinel structure, characterized by a cubic lattice arrangement, wherein lithium ions occupy tetrahedral *8a* sites and titanium ions reside in octahedral *16d* positions.[14] Only 60% of Ti^{4+} is reduced to Ti^{3+} in the LTO structure when it is cycled in its typical voltage window (*ca.* 1.0–3.0 V *vs.* Li/Li^+). However, the LTO structure can take more Li^+ ions if Ti^{4+}/Ti^{3+} is fully utilized.[20]

Despite extensive investigations of over-lithiated LTO electrodes, there are conflicting reports about the chemo-mechanical deformations in the LTO electrodes when over-lithiated. Previous *ex situ* and *in situ* X-ray diffraction studies reported lattice parameters and unit volume changes when $Li[Li_{1/3}Ti_{5/3}]O_4$ was lithiated to $Li_2[Li_{1/3}Ti_{5/3}]O_4$ (between 1.0 and 3.0 V) and when it was over-lithiated to $Li_{2+x}[Li_{1/3}Ti_{5/3}]O_4$ (<1.0 V). Wagemaker reported about a 0.07% change in the lattice parameter of $Li[Li_{1/3}Ti_{5/3}]O_4$ when cycled between 1.0 and 3.0 V.[21] Later, Rui Ma *et al.* reported a decrease in the unit cell volume of $Li[Li_{1/3}Ti_{5/3}]O_4$ (583.481 Å) with lithiation to $Li_2[Li_{1/3}Ti_{5/3}]O_4$ (582.664 Å) and $Li_{2.5}[Li_{1/3}Ti_{5/3}]O_4$ (581.263 Å), which indicates contractions in the unit volume of about 0.14 and 0.38%, respectively.[22] Imazaki *et al.* reported a 0.5% increase in lattice dimension in the LTO structure when cycled between 0 and 1 V *vs.* Li.[23] A neutron diffraction study, supported by DFT calculations, reported that the $Li[Li_{1/3}Ti_{5/3}]O_4$ unit cell is 0.18% greater than $Li_2[Li_{1/3}Ti_{5/3}]O_4$ and 1.08% smaller than $Li_{2.33}[Li_{1/3}Ti_{5/3}]O_4$. The expansion in the unit volume was attributed to the increase in Ti–O bonds due to the reduction of Ti during over-lithiation.[20] Atomic force microscopy (AFM) and multi-beam optical stress sensor (MOSS) were employed to investigate mechanical deformations in the LTO electrode when over-lithiated. The AFM study reported an increase in the electrode volume upon polarization below 1.0 V *vs.* Li, and it was attributed to the decomposition of the electrolyte species.[24] On the other hand, the MOSS study reported large compressive stress generation in the LTO electrode when over-lithiated, and the absolute magnitude of the stress was almost 10-fold greater when over-lithiated (<1.0 V) compared to lithiation around 1.5 V *vs.* Li. This massive stress was attributed to the formation of metastable phases in the electrode structure.[25]

Three outstanding questions remain to be addressed: (1) can LTO still be defined as a zero-strain electrode when over-lithiated? (2) How much do the LTO electrodes deform when over-lithiated?; and (3) how much are the deformations reversible and irreversible when LTO is cycled at lower voltages? In this study, we utilized digital image correlation to probe *operando* electrochemical strain generation in the LTO electrode during cycling. When cycled between 1.0 and 3.0 V, the LTO electrodes underwent a negligible amount of strain generation (*ca.* 0.05%) during Li insertion/removal. However, when the LTO was overlithiated by polarization until 0.35 V *vs.* Li, the electrode experienced a tremendous amount of positive strain (*ca.* 0.8%). The absolute magnitude of strain generation at lower voltages (<1.0 V) was approximately ten times greater compared to the typical voltage range (between 1.0 and 3.0 V). Furthermore, when cycled between the 0.35 and 3.0 V voltage window, the electrode experienced a significant amount of irreversible strain generation. We hypothesized that both structural instabilities and the formation of solid-electrolyte interface (SEI) layers contribute to large mechanical deformations when over-lithiated at lower voltages (<1.0 V). *Operando* stress measurements and *ex situ* X-ray photoelectron spectroscopy measurements were further conducted to better understand the deformation mechanisms in the LTO electrodes.

Experimental

Electrode preparation

The LTO composite electrode was prepared by first mixing sodium carboxymethyl cellulose (binder) and water (solvent) in a 1 : 40 ratio (mass basis). The binder : solvent mixture was homogenized using a Thinky centrifugal mixer for 10 minutes

at 3000 rpm. After homogenization, both LTO (active material) and SuperP (conductive carbon) were added to the solution in an 8 : 1 ratio (mass basis). The final active material conductive carbon : binder : solvent ratio was 8 : 1 : 1 : 40 (mass basis). The slurry was mixed in the centrifugal mixer for 30 minutes at 3000 rpm. For strain measurements, the slurry was blade-cast onto aluminum foil. Once dried, the free-standing electrodes were obtained by peeling the electrode from the aluminum foil, and then, they were cut into rectangular shapes for strain measurements. The thickness of the free-standing composite electrode was about 125 μm (SI Fig. S1A). For stress measurements, the slurry was cast onto the rough side of a single-sided polished silicon wafer (480 μm thick) using a doctor blade. The composite electrode thickness on the substrate was about 20 μm (SI Fig. S1B).

Electrochemical cycling

$LiClO_4$ salt, dimethyl carbonate (DMC, anhydrous, >99%) solvent, and ethylene carbonate (EC, anhydrous, 99%) solvent were purchased from Sigma Aldrich. The electrolyte was prepared by dissolving 1 M $LiClO_4$ in a 1 : 1 (V : V) ratio of EC : DMC solvents. There was a 24 h resting period prior to electrochemical cycling. Initially, the electrode was cycled between 1.0 and 3.0 V at a 50 μV s^{-1} scan rate for five cycles; then, the voltage window was increased to the 0.35–3.0 V range in the subsequent cycles. The electrode was cycled at a relatively slow scan rate (50 μV s^{-1}) to minimize transport limitations and ohmic effects.

Operando strain measurements

Details of the experimental setup for *operando* strain measurements were discussed in our previous publication.[26] After custom cell assembly, images of the electrode were captured periodically by using a high-resolution Grasshopper3 5.0 MP optical camera with a 12.0× adjustable zoom lens. Images were captured every two minutes during electrochemical cycling and every ten minutes during open-circuit rest. Displacement and strain generation were computed using Vic2D software with a step size of 15 and a subset size of 111 × 111 pixels. The area of interest was 750 μm in width and 500 μm in height. Horizontal normal strain, ε_{xx}, and the electrochemical data were synchronized using custom MATLAB software. The normal strain, ε_{xx}, was reported as a percentage (%), and positive strains indicate volumetric expansion of the composite electrode.

Operando curvature measurements

Stress–thickness measurements were carried out using a multi-beam optical stress sensor equipment (kSA MOS, k-Space Associates, Inc., USA). A detailed description of the custom electrochemical cell and the experimental technique can be found in our previous publications.[27–29] The curvature change of the electrode substrate, denoted as $\Delta\kappa$, was calculated using the formula: $\Delta\kappa = \frac{d(t) - d_i}{d_i}\frac{\cos(\alpha_i)}{2ln}$, where d_i is the initial distance between the beams and $d(t)$ is the distance between the beams at time t. The distance between the CCD camera and the substrate is represented by l, the refractive index of the solution is represented by n, and the incident angle is represented by α_i.[30] In this study, 1 M $LiClO_4$ in EC : DMC solution was used as the electrolyte, with a refractive index of 1.409.[29] The curvature change was used in the Stoney equation to calculate the force exerted on the substrate during electrochemical cycling. The Stoney equation is $F = \frac{Eh_s^2K}{6(1-\nu)}$, where F is the in-plane force through the width of the film, E is the substrate's Young's Modulus (140 GPa for silicon wafer), h_s is the substrate thickness (480 μm), ν is the Poisson's ratio of the substrate (0.265), and K is the resulting curvature of the substrate. The force is the stress-thickness product in the composite electrode with units of N m^{-1}. A lab-developed MATLAB code was used to synchronize the electrochemical data with the stress-thickness values.

X-ray photoelectron spectroscopy (XPS) Measurements

X-ray photoelectron spectroscopy (XPS) was performed to examine the surface composition and chemical states of elements in as-received and oxidized samples as a function of depth. The measurements were conducted using a Nexsa ThermoFisher Scientific spectrometer equipped with a monochromatic Al Kα X-ray source (1486.6 eV, 72 W) and a spherical mirror analyzer set to a 50 eV pass energy. The XPS data were collected using a 400 μm diameter X-ray beam, with photoelectrons detected perpendicular to the sample surface. During analysis, the chamber pressure was maintained at ~5 × 10^{-9} Torr, and the spectra were charge-referenced to the C 1s peak at 284.8 eV. Peak fitting and quantification were performed using CasaXPS software with a Shirley background correction. Depth profiling was carried out using 300 eV mono-energetic argon ion sputtering over a raster area of 1.2 mm × 1.2 mm. XPS measurements were then taken at the center of the sputtered region using a 400 μm X-ray beam. Sputter rates were calibrated using Ta_2O_5 as the reference material.

Results and discussion

Morphological and structural characterization

Fig. 1A shows the scanning electron microscopy image of the LTO powders, and the particle size ranges from 0.1 to 0.6 micrometers (Fig. 1B). The crystalline structure of the LTO powders was investigated by conducting X-ray diffraction measurements (Fig. 1C). The Bragg peaks of the LTO powders are located at 35.5, 37.3, 43.2, 47.3, 57.1, 66.0 and 67.8°, which correspond to (311), (222), (400), (331), (511), (440), and (531) planes, respectively. The X-ray patterns align well with JCPDS card No-26-1198 for $Li[Li_{1/3}Ti_{5/3}]O_4$.[22]

Operando mechanical measurements were performed to investigate strain generation in lithium titanate ($Li[Li_{1/3}Ti_{5/3}]O_4$, LTO) composite electrodes during electrochemical cycling using the digital image correlation method (Fig. 2A). The LTO

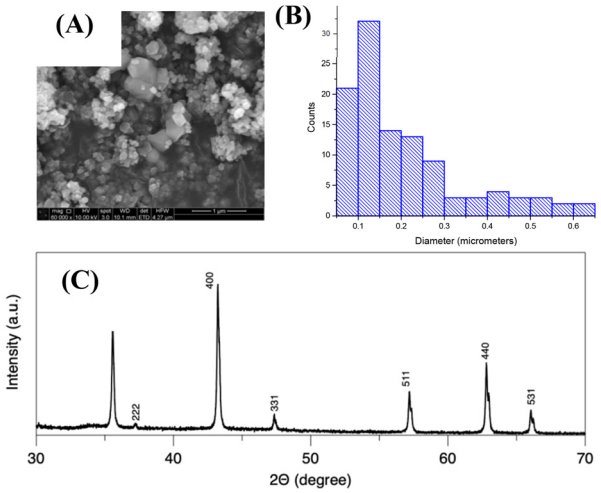

Fig. 1 Morphological and structural characterization. (A) Scanning electron microscopy image of the LTO powders, (B) particle size analysis of the LTO powders, and (C) X-ray diffraction patterns of the LTO powder.

electrode was cycled between a typical voltage range, 1.0–3.0 V (*vs.* $Li/Li^{0/+}$) *via* cyclic voltammetry at 50 μV s^{-1} in 1 M $LiClO_4$ in EC : DMC electrolyte for the first five cycles. During the typical voltage window in the first five cycles, the electrochemical strain, ε_{xx}, varied within 0.07 to −0.07% as Li ions were inserted/removed into the LTO electrode in a typical voltage window. The cumulative strain at the end of the fifth cycle was almost zero, indicating the high reversibility of the mechanical deformations. Then, the operational voltage was changed to a lower voltage range, 0.35 to 3.0 V, for the subsequent two cycles. The electrode underwent a significant amount of deformation, up to 0.8% at lower voltages. Furthermore, the cumulative strains at the end of the 6^{th} and 7^{th} cycles were about 0.26 and 0.38%, respectively, indicating the generation of a significant amount of irreversible deformation in the electrode.

Mechanical deformations in the 1.0–3.0 V range

Current evolution and strain changes were plotted against voltage in Fig. 2B to better understand the governing forces behind mechanical deformation during the typical voltage window (1.0–3.0 V). Lithiation occurs in LTO anodes during charging, and delithiation takes place during discharging. A single current peak was observed at around 1.45 and 1.68 V, during lithiation and delithiation cycles, respectively. In the literature, a single current peak at around 1.55 V was associated with the two-phase transformation between $Li[Li_{1/3}Ti_{5/3}]O_4$ and $Li_2[Li_{1/3}Ti_{5/3}]O_4$. The phase transformation was expressed as the Li-ion movement between octahedral *16c* sites and tetrahedral *8a* sites in the crystal lattice.[9,31] Associated strain evolution in the LTO electrode during the first five cycles is plotted in Fig. 2B. The strain change value was set to zero at the beginning of each cycle for better demonstration. There were almost no mechanical deformations during the early period of lithiation. The electrode expanded slightly (~0.03%) between ~1.70 and 1.48 V. Then, the electrode contracted suddenly (up to −0.05%) between 1.48 and 1.41 V. At the lower voltages during lithiation, the electrode almost reached zero strains. A similar deformation behaviour was also recorded during the delithiation cycles. Initially, there was a negative strain generation up to −0.06% until about 1.50 V, followed by expansion up to 0.02% around 1.70 V. There was almost no mechanical deformation at voltages higher than 1.70 V during delithiation. An *operando* XRD study in the literature reported an initial increase in lattice volume (ΔV) during the early period of lithiation, followed by a reduction at the later stages of the lithiation.[32] The change in the lattice volume in the *operando* XRD study aligns very well with the recorded electrochemical strain behaviour in our study. It is quite impressive that the macroscale DIC technique was able to detect such small deformations in the LTO composite electrode.

Strain derivatives were calculated by taking the derivative of strain with respect to voltage values (Fig. 2C). Previous mechanical measurements on battery electrodes demonstrated a correlation between phase-induced nano-scale deformations in the lattice and the micro-scale mechanical deformations in electrodes for Li-, Na-, K-, and Zn-ion batteries.[26,33–35] A single-strain derivative peak was observed at around 1.45 and 1.68 V during lithiation and delithiation cycles, respectively. SI Fig. S2 shows the current evolution and associated stress derivatives, measured *via* the MOSS system. A single stress derivative was recorded for lithiation and delithiation cycles at around 1.45 and 1.68 V, respectively. The locations of both strain- and stress-derivative peaks were in close alignment with the location of the current peaks, within ±0.03 V. The close correlation further indicates the phase-transformation-induced mechanical deformations in the LTO electrode.

Deformations under over-lithiation (<1.0 V)

SI Fig. S3 shows the current evolution and strain generation in the LTO when cycled between 0.35 and 3.0 V. The strain values were set to zero at the beginning of the 6^{th} and 7^{th} cycles to better demonstrate the deformation behaviour. Similar to previous cycles, there was a single current peak during lithiation cycles at around 1.48 V. Strain generation was similar to the previous cycles until the voltage reached 1 V. Then, the current began to decay, and there was a tremendous expansion in the electrode at voltages lower than 1.0 V. During the subsequent delithiation cycles, there was a small current peak located at around 0.45 V, followed by a dominant current peak located at 1.68 V. The volume of the electrode contracted during the initial period of the delithiation until about 1.50 V. After cycling between a 0.35 and 3.0 V window, the volume of the electrode did not come back to its original state, resulting in irreversible strain generation in the electrode. The similar expansion-contraction behaviour between cycles 6 and 7 indicates the partially reversible deformations on the electrode structure upon Li insertion/extraction. The generation of irreversible strains at the end of cycles 6 & 7 suggests the formation of solid-electrolyte interphase (SEI) layers at lower voltages (<1.0 V).

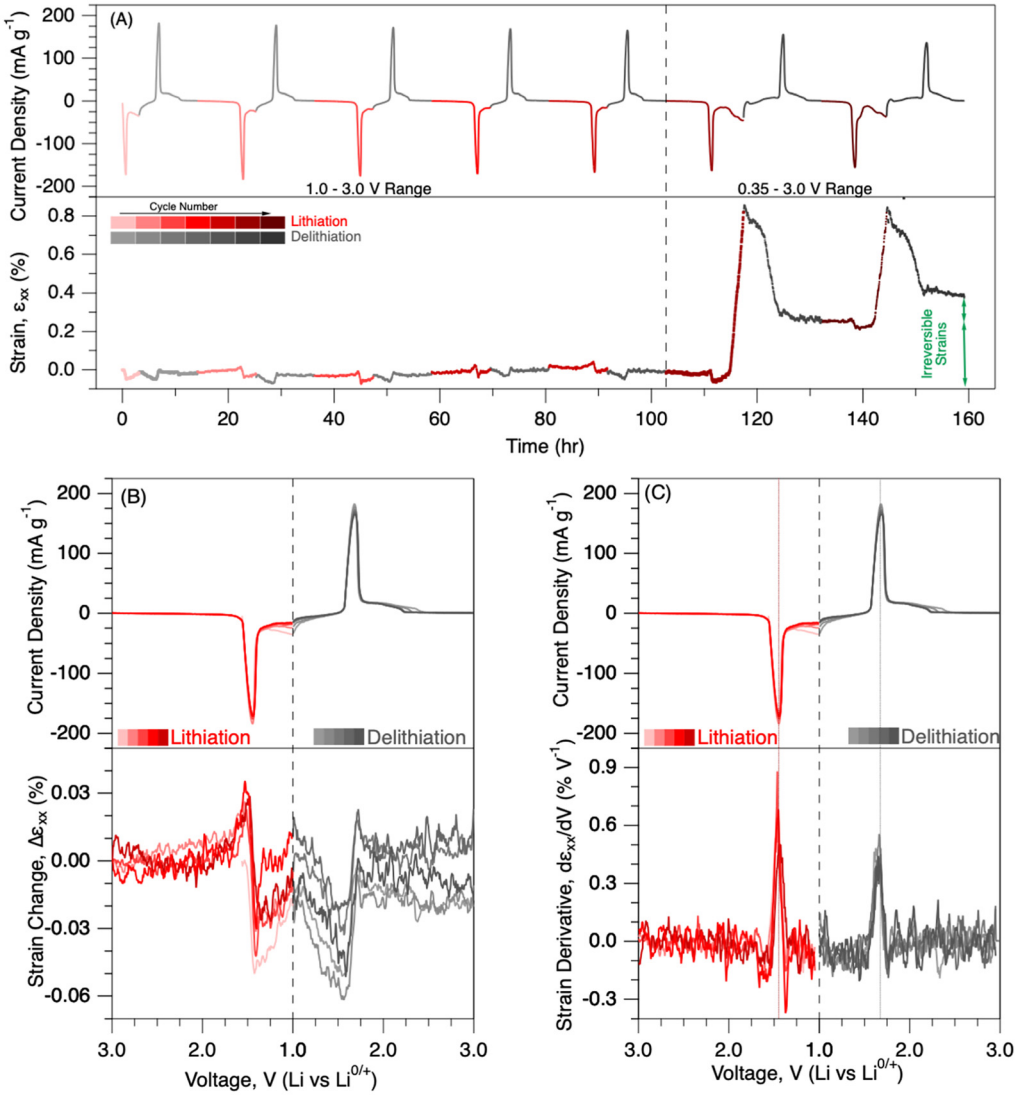

Fig. 2 Mechanical deformations in the LTO composite electrode. (A) Current generation (top) and strain evolution (bottom) with respect to time are shown at a 50 μV s^{-1} rate. The electrode was cycled between 1.0 and 3.0 V (*vs.* Li/Li$^{0/+}$) for five cycles, followed by 0.35–3.0 V (*vs.* Li/Li$^{0/+}$) in the subsequent cycles. The vertical dashed line marks the end of the fifth cycle. Green arrows indicate the irreversible strain generations. (B) Strain changes and (C) evolution of strain derivatives during discharge and charge during the initial five cycles. Strains were set to zero at the beginning of each discharge for better comparison in (B).

The LTO electrode contracted by about 0.05% when cycled in a typical voltage window between 1.0 and 3.0 V during discharge. On the other hand, the electrode expanded almost to 0.8 and 0.5% by the 6th and 7th discharge at 0.35 V (Fig. 3A). Therefore, there were about tenfold more deformations in the electrode when over-lithiated (higher state-of-charge) until 0.35 V compared to the typical voltage window. Strain derivatives were calculated to shed light on deformation mechanisms at over-lithiation. There are three strain-derivative peaks in Fig. 3B. The first strain derivative peak is positive at around 1.45 V, similar to the ones when the electrode was only cycled between 1.0–3.0 V (Fig. 2C). There are two more strain derivatives with negative magnitude at around 0.70 and 0.45 V. The appearance of additional strain derivatives at lower voltages may be associated with the phase transformation due to further lithiation in the structure and the formation of SEI layers. Interestingly, Yan-Bing He *et al.* also observed irreversible current generation at around 0.70 V when LTO was lithiated in the $LiPF_6$ EC : DMC electrolyte, and FT-IR measurements indicated the formation of SEI layers due to electrolyte decomposition.[36] The digital image correlation measurements were able to detect the formation of SEI/CEI layer-induced mechanical deformations in battery electrodes, such as graphite anodes and lithium iron phosphate cathodes.[37–39] Therefore, the strain-derivative peak at 0.70 V was attributed to the decomposition of the electrolyte species on the LTO surface. *In situ* XRD studies[32] reported an increase in the lattice unit volume of the LTO electrode at around 0.50 V upon

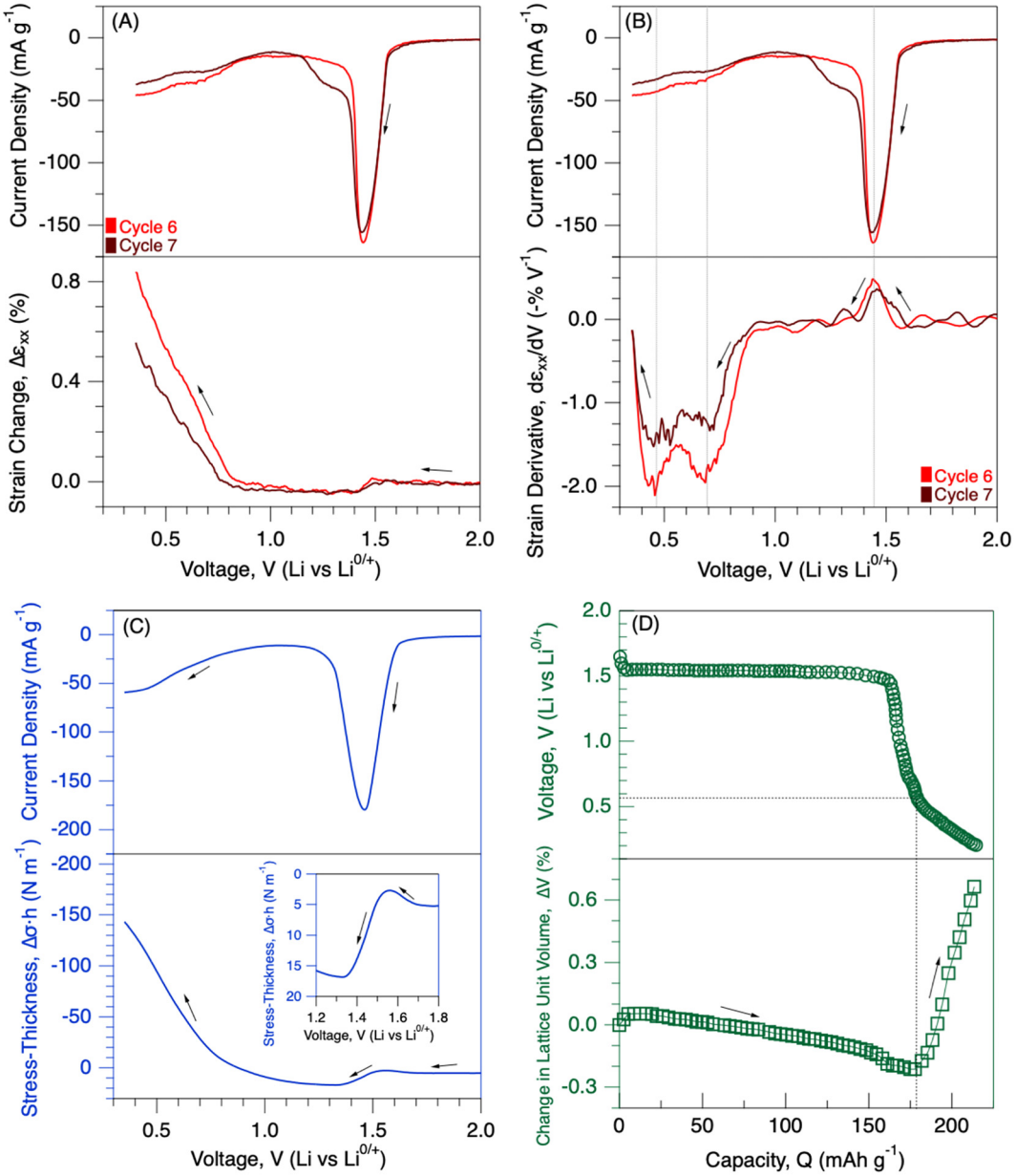

Fig. 3 Mechanical deformations under over-lithiation. (A) Strain generation and (B) strain derivatives in the LTO composite electrode during lithiation until 0.35 V at a 50 μV s^{-1} rate. Data are collected from Fig. 2. (C) Stress generation in the LTO composite electrode, measured using MOSS, during lithiation until 0.35 V at a 50 μV s^{-1} rate. (D) Voltage and change in the lattice unit cell volume of the LTO electrode. Data are extracted from the XRD study conducted by Uyama *et al.*, Energy Storage Materials, 2022.

over-lithiation (Fig. 3D); therefore, the strain-derivative peak at 0.45 V was attributed to the lattice changes in the electrode.

Fig. 3C shows the stress generation in the LTO electrode when polarized until 0.35 V during lithiation. Initially, there is no significant stress generation until the potential reaches ~1.65 V. The LTO electrode experienced a slight compression, followed by tensile stress generation (subwindow in Fig. 3C). At the same period, strain measurements indicated slight expansions, followed by contractions in the electrode (Fig. 2B). Then, there was a significant amount of compressive stress generation at higher-state-of-discharge (<1.0 V). At a similar potential, the strain measurements demonstrated large expansions in the electrode as well (Fig. 3A). Stress and strain generations were also plotted in SI Fig. S4 for better demonstration. Similar to strain measurements, there was almost a tenfold increase in the absolute magnitude of the stress generation at lower voltages (<1.0 V) compared to the typical voltage window (between 1.0 and 3.0 V). Overall, both the electrochemical and mechanical responses of the LTO electrode were consistent between stress and strain measurements. The significantly larger deformations at lower voltages may be associated with both the phase transitions in the electrode structure and the formation of SEI layers.

Recently, Uyama *et al.* employed *operando* XRD and X-ray absorption studies to shed light on these discrepancies at lower voltages (<1 V).[32] According to their study, a two-phase reaction takes place in LTO between a 1.0 and 3.0 V window, and the electrode undergoes a one-phase reaction below 1.0 V upon over-lithiation. The one-phase reaction is defined when $Li_2[Li_{1/3}Ti_{5/3}]O_4$ is transformed into $Li_{0.21}$ $Li_2[Li_{1/3}Ti_{5/3}]O_4$ upon further lithiation. We extracted electrochemical and structural data from their study and plotted them in Fig. 3D. The volume of the lattice unit cell decreased about 0.2% during the two-phase reaction, followed by an increase in the lattice of up to 0.66% at lower voltages. Their XAS and XRD studies indicated reversible changes in the bond length of titanium and oxygen atoms.[32] The direction of unit volume change in their study aligns well with our mechanical measurements. Positive strain and compressive stress generation shown in Fig. 3 align well with the increase in volume of the lattice unit cell at lower voltages (<1.0 V). However, the relative absolute changes in the lattice unit cell were about 3–4 times greater when over-lithiated compared to a 1.0–3.0 voltage window. In our mechanical measurements, there is almost a tenfold increase in the absolute magnitude of stress and strain generations at lower voltages (<1.0 V) compared to the typical voltage window (between 1.0 and 3.0 V). Therefore, the formation of SEI layers must also contribute to the additional mechanical deformations at the lower voltages.

The chemical composition of the SEI layers was investigated *via* XPS measurements after the electrode was lithiated to 0.5 V. The area of the XPS measurement was also etched for 60 and 500 seconds to investigate the depth profile of the SEI chemistry. Spectral components were fitted using CasaXPS (v.2.3.24) with a mixed Gaussian–Lorentzian line shape to determine peak positions and full width at half maximum (FWHM) values. Each peak was assigned and constrained based on the known chemical composition and structure of the material and on literature binding energies of the constituent elements. Although the residual standard deviation (RSD) values are relatively high (~1.8), the peak model is chemically justified and reproduces the experimental spectra without systematic features in the residuals, in line with the approach discussed in the literature.[40]

Investigation of C 1s and O1s spectra sheds light on the chemistry of the SEI layers. In the C 1s spectra, there are five distinct peaks at various etching periods. The peak at 283.3 eV is assigned to the sp2 C=C bonds in the conductive carbon. The intensity of the conductive carbon peak also increases with surface etching time, indicating that the conductive carbon was covered by the SEI layers during cycling.[41,42] The peak at 284.8 eV is associated with the presence of the hydrocarbons. The peak at 286.4 eV is ascribed to C–O/C–OH bonds, which may be due to either the presence of the CMC binder or the organic chemical species in the SEI layers. The peak at 288.4 eV is assigned to the presence of O–C–O/C=O bonds and the carboxylic group (O–C=O).[41–43] The peak at 290 eV is attributed to the Li_2CO_3 and Li alkyl carbonates. In the O 1s spectra, there are four distinct peaks at various etching periods. The peak at 530.3 eV is assigned to O^{2-} anions in the LTO structure.[42] The peak intensity increases with surface etching time, indicating that LTO powders were covered by the SEI layers with cycling. The peak at 531.4 eV is attributed to the presence of LiOH on the surface. The peak at 532.0 eV is associated with the Li_2CO_3 and Li alkyl carbonates. The peak at 533.1 eV is attributed to O–C–O/C=O bonds from the binder as well as the formation of carbon singly bonded to oxygen (C–O) and Li_xPO_y.[42] Overall, the intensity of conductive carbon and LTO peaks increases with the surface etching time, demonstrating the presence of the thick-SEI layers after polarizing to 0.5 V.

Predicted strains in composite LTO electrodes

We calculated predicted strains in the composite LTO electrode using a mathematical model. The model only considers elastic deformation associated with the unit lattice change in the LTO particles. The model does not incorporate the plastic deformations and the formation of solid-electrolyte interphase (SEI) layers into account. The model was previously developed by E. Jones *et al.* to predict strain generation in the composite graphite electrodes for Li-ion batteries. There was a close correlation between experimentally measured strains and predicted strains.[44] Later, our group has also utilized the model to predict strains in $LiMn_2O_4$ and $NaFePO_4$ cathodes for Li-ion and Na-ion batteries, respectively. The predicted strains aligned well with the electrochemical strains at slower rates.[45,46] Shortly, the effective bulk modulus of the porous network, K_{pm}, was calculated *via* open cell theory.[47] The bulk modulus of the complete LTO composite electrode, K_{ce}, was computed by applying the S-combining rule.[48] By using these elastic properties, strain generation in the composite LTO electrode was predicted using

$$\varepsilon_{ce} = \varepsilon_{LTO}\phi_{LTO} + \left(\frac{\varepsilon_{LTO}}{\frac{1}{K_{pm}} - \frac{1}{K_{LTO}}}\right)\left(\frac{1}{K_e} - \frac{1}{K_{average}}\right)$$

The details of the model are discussed briefly in the SI. Governing equations and the parameters in the model are listed in SI Tables S1–S4. ε_{LTO} is the linear strain of the LTO particles due to lithium intercalation. ε_{LTO} was calculated using the XRD data in Fig. 3D and assuming isotropy.

Fig. 5 shows the predicted strains plotted alongside the experimentally measured strains. The strain generation at higher voltages (between 1.0 and 3.0 V) resembles each other, indicating that the strains are generated due to unit lattice changes in the electrode during lithium intercalation. This alignment between predicted and measured strains also further demonstrates reversible elastic deformations in the electrode (Fig. 2B). However, the predicted strains largely deviate from the experimentally measured strains at lower voltages (<1.0 V *vs.* Li). The predicted strains are about 0.12% at lower voltages, whereas the electrode experienced about 0.83% and 0.55% strains during the sixth and seventh discharge cycles at lower voltages. If the strains were primarily generated

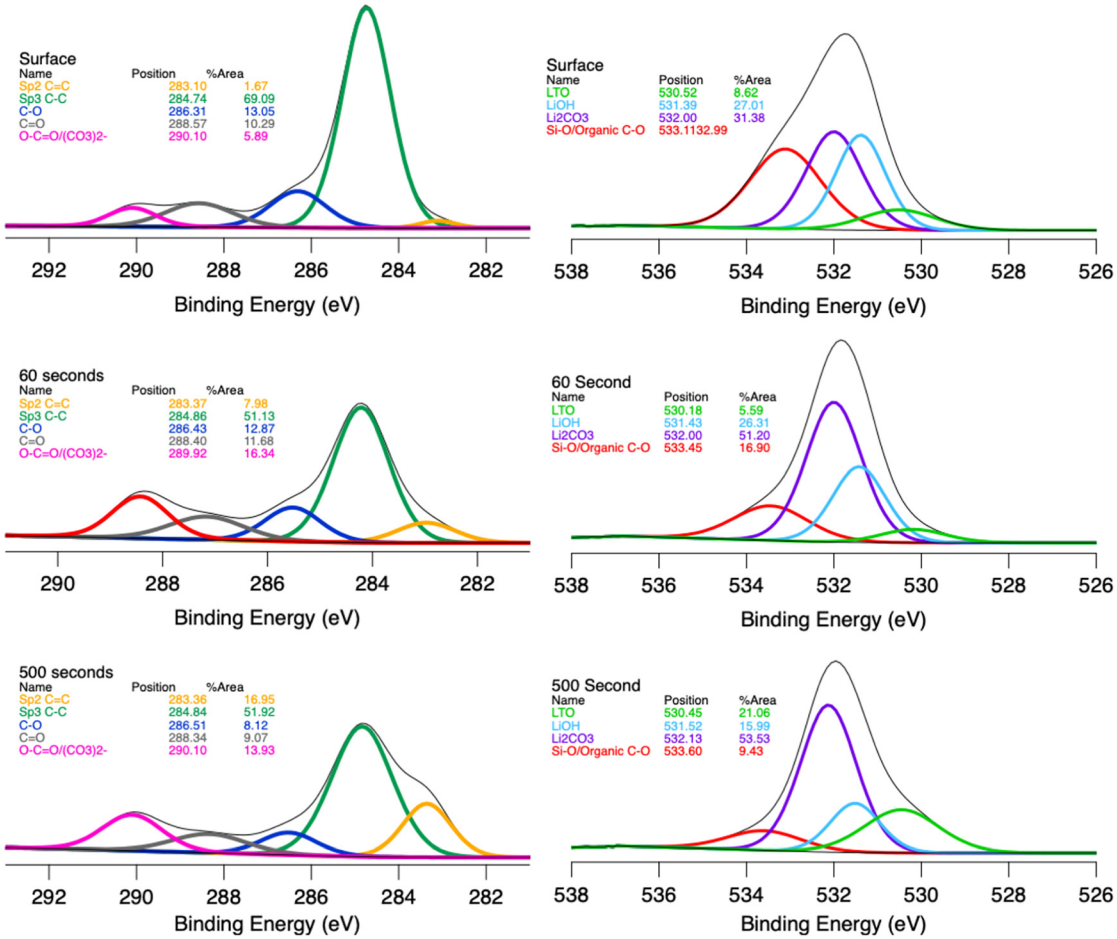

Fig. 4 Surface chemistry analysis. X-ray photoelectron spectroscopy measurements of the composite LTO electrode, lithiated until 0.5 V. The left side shows the C 1s spectra and the right side shows the O 1s spectra. The surface was etched for 60 and 500 seconds after the surface data were collected.

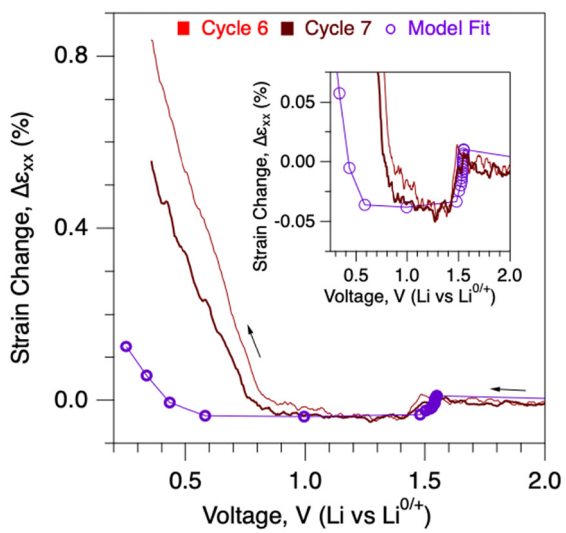

Fig. 5 Predicted strains in the composite LTO electrode. Electrochemically measured strains during the 6th (bright red) and 7th (darker red) discharge cycles are plotted on top of the predicted strains in the composite LTO electrode (purple).

due to elastic deformations in the unit structure of the LTO due to Li intercalation, similar strain generation would be expected between the experimentally measured and predicted strains at lower voltages. The large deviation suggests the additional strains generated due to SEI layer formation on the LTO particles.

Discussion on Li-intercalation *vs.* SEI-layer formation-induced mechanical deformations at lower voltages

Operando mechanical measurements in Fig. 3 demonstrate large mechanical deformations when the electrode is cycled below 1.0 V. The relative magnitude of the deformations below 1.0 V is significantly higher than the deformation when the electrode cycled between the 1.0–3.0 V zone. Previous XRD measurements indicated large expansions of the unit lattice when the electrode was over-lithiated (below 0.5 V). At the same time, *ex situ* XPS analysis in Fig. 4 demonstrates the formation of the SEI layer on the LTO particles, which contributes to positive strain generation in the composite electrode. Therefore, both expansions in the unit structure of the LTO particles and the formation of SEI layers on the surface of the

LTO particles contribute to the mechanical deformations at lower voltages. However, a key question remains mysterious: how much structural distortion *vs.* surface instabilities are responsible for the mechanical deformations at lower voltage windows?

We tabulated the strain generation in various voltage windows during the 6th and 7th cycles in SI Tables 6 and 7. XRD measurements indicated that most of the phase transformation-induced structural deformations take place below 0.5 V. In this period, the predicted strains were about 0.12%. The experimentally measured strains below 0.5 V are about 0.35% and 0.24% during the 6th and 7th cycles. If we assume that redox reactions only induced crystalline changes in the electrode structure at lower voltages, then the predicted strains would correspond to lithium intercalation-induced mechanical deformations in the composite electrode. Unfortunately, to our knowledge, there is no available data in the literature about the reversibility of the over-lithiated phase of the lithium titanate. The current evolution and corresponding strain changes during the 6th and 7th charge cycles are plotted in Fig. 6. There is a current peak during the early period of delithiation, and the current almost reaches zero at around 1.1 V. The strain change between 0.35 and 1.1 V is about −0.17 and −0.15% during the 6th and 7th delithiation cycles, respectively (SI Table S6). The magnitude of the experimentally measured mechanical deformations during this period is almost similar to the predicted strains during over-lithiation below 0.5 V. Then, during over-lithiation below 0.5 V, additional strain generation in the experimental measurements is likely to be associated with the formation of SEI layers.

The question remains for the strains generated between 0.8 and 0.5 V during the discharge cycles. There were about 0.48% and 0.32% strain generation in this voltage window during the 6th and 7th lithiation cycles, respectively. XRD measurements indicated that there is a negligible amount of change in the crystalline structure of the electrode. In this period, there is a small amount of current generation in the electrochemical response (Fig. 3A). An electron energy loss spectroscopy study in the literature reported a spontaneous charge transfer process of $Ti^{3+} \rightarrow e^{-} + Ti^{4+}$ in the fully lithiated phase of lithium titanate.[49] The generated electrons in the spontaneous reaction could lead to decomposition of the organic molecules in the electrolyte and the formation of SEI layers. Ti^{4+} of the LTO is also reported to have a catalytic effect on the dehydrogenation and decarbonylation of alkyl carbonate solvents, which produces organic SEI layers and the formation of CO_2, CO, and H_2 gases.[50,51] The gas formation could also lead to swelling of the LTO composite electrode.[52] Therefore, the mechanical deformation in the voltage between 0.5 and 0.8 V during lithiation could be linked to the formation of SEI layers on the surface of the electrode and swelling of the composite electrode. This also aligns well with the strain derivative analysis shown in Fig. 3.

There is a still puzzling fact about mechanical deformations during delithiation after over-lithiation. 0.55% and 0.43% of the strains were reversible within the sixth and seventh cycles, respectively. The irreversible strains within the cycles of the sixth and seventh were only about 0.28% and 0.12%, respectively. The reduction in irreversible strain in the subsequent cycle indicates saturation of SEI growth on the electrode. Fig. 6 shows that a large amount of the strain relaxes during the subsequent delithiation process between 1.1 and 1.55 V. It is unlikely that strain generations are governed by any electrochemical reactions since the current generation is almost negligible in this period. It also rules out the delithiation-induced strain generation in this voltage window. We speculate that this may be associated with the removal of organic-rich loosely bound SEI components from the surface of the electrode, either due to dissolution or mechanical fracture of loosely bound SEI components. Unfortunately, there is not much known in the literature about either the stability of SEI layers, gas evolution, or structural changes in the crystalline structure of the lithium titanate during delithiation after over-lithiation. Our study demonstrated puzzling facts about complicated mechanical deformations in the lithium titanate when over-lithiated.

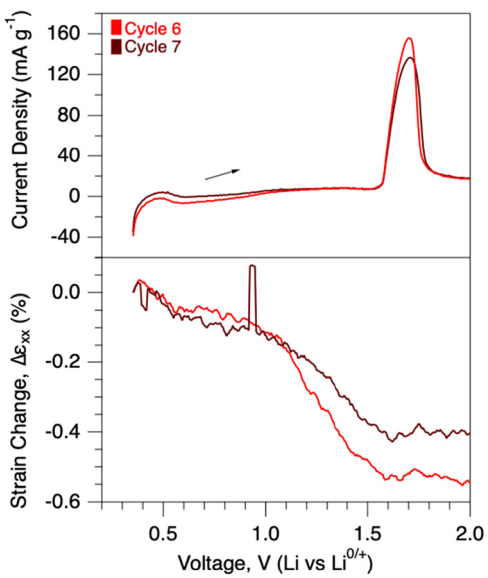

Fig. 6 Mechanical deformations during charge after overlithiation. Strain generation in the LTO composite electrode during the 6th and 7th delithiation cycles. Data are collected from Fig. 1. Strain was set to zero at the beginning of the delithiation cycle.

Conclusion

Mechanical deformations in the LTO electrodes were investigated by conducting *operando* stress and strain measurements in various voltage windows. When cycled between 1.0 and 3.0 V voltage windows, the electrode experiences almost negligible mechanical deformations during cycling, and the deformations are predominantly elastic since irreversible strains are almost negligible at the end of each cycle. Strain and stress derivatives demonstrated a single peak during each charge/discharge cycle, which aligns well with the location of the current

peak, indicating the phase-induced elastic deformations in the structure. When cycled between 0.35 and 3.0 V voltage windows, the electrode experiences a significant amount of expansion during over-lithiation and large negative strain generation during the subsequent delithiation. *Operando* stress measurements further verified the large mechanical deformations observed by *operando* strain measurements. The electrode did not turn back to its original mechanical state, resulting in plastic deformations when cycled between 0.35 and 3.0 V. Two additional strain derivatives at 0.70 and 0.45 voltages were associated with the formation of a solid-electrolyte interphase and the structural changes in the unit volume upon Li insertion, respectively. XPS measurements exhibited the formation of SEI layers on the LTO electrodes when cycled at lower voltages. Lithium intercalation-induced electrochemical strains were predicted based on a mathematical model and unit-lattice changes from XRD data in the literature. The predicted strains matched well with the experimentally measured strains between 1.0 and 3.0 V voltage windows. However, in a higher state of discharge below 1.0 V, there is a large deviation between predicted strains and experimentally measured strains. The deviation was attributed to the formation of SEI layer-induced mechanical deformations, especially between the 0.5 and 0.8 V window, where there is a negligible amount of crystallinity changes reported from XRD studies. Our study provides an in-depth examination of the chemo-mechanical deformations in the LTO electrode under over-lithiated conditions.

The key highlights in the study are as follows: the LTO composite electrode undergoes a negligible amount of deformation when cycled between the 1.0 and 3.0 V regime. However, the LTO composite electrodes undergo large deformations below 1.0 V. Irreversible deformations significantly increased when the electrode was cycled in a wider voltage window (0.35–3.0 V). The asymmetric behavior between experimentally measured strains and predicted strains based on XRD data between 0.8 and 0.5 V during lithiation indicates SEI-induced deformations. Interestingly, during the subsequent delithiation cycles after overlithiation, the composite electrode relieved a significant amount of strains in the voltage periods of 1.1–1.55 V, where there was a negligible amount of current generation. We suggest that the battery community pay attention to better understand structural, mechanical and chemical instabilities in the lower voltage windows of LTO electrodes, including the subsequent delithiation period. Our study demonstrated that the LTO does not behave as a "zero-strain" electrode when cycled below 1.0 V and the large deformations were associated with complicated surface and structural instabilities. We anticipate that this methodology can also be applied to investigate deformation mechanisms in other zero-strain electrodes in elevated states of (dis)charge.

Author contributions

Ö. Ö. Ç. conceived the idea and supervised the work. B. B. and B. Ö. performed the strain and stress measurements and data analysis, respectively. M. L., B. M. S. and X. L. performed and analyzed the XPS measurements. All authors discussed the results. The authors declare that they have no competing interests.

Conflicts of interest

There are no conflicts to declare.

Data availability

The data supporting this article have been included as part of the supplementary information (SI). Supplementary information: optical images of the electrodes, stress derivatives, strain evolution, strain *vs.* stress comparison figures, and mathematical models. See DOI: https://doi.org/10.1039/d6eb00040a.

Acknowledgements

All *operando* strain, stress, and electrochemical measurements were carried out at Oklahoma State University and supported by the U.S. Department of Energy, Office of Science, Basic Energy Sciences (Award number DE-SC0021251). V. M. acknowledges funding from the Joint Center for Energy Storage Research, an Energy Innovation Hub funded by the U. S. Department of Energy, Office of Science, Basic Energy Sciences.

References

1 K. Zhao, M. Pharr, J. J. Vlassak and Z. Suo, *J. Appl. Phys.*, 2010, **108**, 073517.
2 D. J. Miller, C. Proff, J. G. Wen, D. P. Abraham and J. Bareño, *Adv. Energy Mater.*, 2013, **3**, 1098–1103.
3 S. K. Mulpuri, B. Sah and P. Kumar, *iScience*, 2023, **26**, 107770.
4 T. Kim, L. K. Ono and Y. Qi, *J. Mater. Chem. A*, 2022, **11**, 221–231.
5 A. Mukhopadhyay and B. W. Sheldon, *Prog. Mater. Sci.*, 2014, **63**, 58–116.
6 Y. Liu, D. Lin, P. Y. Yuen, K. Liu, J. Xie, R. H. Dauskardt and Y. Cui, *Adv. Mater.*, 2017, **29**, 1605531.
7 X. Zhao and G. Ceder, *Joule*, 2022, **6**, 2683–2685.
8 X. Zhao, Y. Tian, Z. Lun, Z. Cai, T. Chen, B. Ouyang and G. Ceder, *Joule*, 2022, **6**, 1654–1671.
9 K. Ariyoshi, R. Yamato and T. Ohzuku, *Electrochim. Acta*, 2005, **51**, 1125–1129.
10 W. Zhang, M. Topsakal, C. Cama, C. J. Pelliccione, H. Zhao, S. Ehrlich, L. Wu, Y. Zhu, A. I. Frenkel, K. J. Takeuchi, E. S. Takeuchi, A. C. Marschilok, D. Lu and F. Wang, *J. Am. Chem. Soc.*, 2017, **139**, 16591–16603.

11 X. Jiang, Z. Zeng, L. Xiao, X. Ai, H. Yang and Y. Cao, *ACS Appl. Mater. Interfaces*, 2017, **9**, 43733–43738.
12 S. Chong, Y. Wu, S. Guo, Y. Liu and G. Cao, *Energy Storage Mater.*, 2019, **22**, 120–127.
13 L. Li, Z. Hu, Y. Lu, C. Wang, Q. Zhang, S. Zhao, J. Peng, K. Zhang, S. Chou and J. Chen, *Angew. Chem.*, 2021, **133**, 13160–13166.
14 S. Chong, J. Yang, L. Sun, S. Guo, Y. Liu and H. K. Liu, *ACS Nano*, 2020, **14**, 9807–9818.
15 Y. Wang, X. Yu, S. Xu, J. Bai, R. Xiao, Y.-S. Hu, H. Li, X.-Q. Yang, L. Chen and X. Huang, *Nat. Commun.*, 2013, **4**, 1–7.
16 E. Lee, B. J. Kwon, F. Dogan, Y. Ren, J. R. Croy and M. M. Thackeray, *ACS Appl. Energy Mater.*, 2019, **2**, 6170–6175.
17 Z. Li, B. Ozdogru, B. Bal, M. Bowden, A. Choi, Y. Zhang, H. Wang, V. Murugesan, V. G. Pol and Ö. Ö. Çapraz, *Adv. Energy Mater.*, 2023, **13**, 2301329.
18 B. Zhao, X. Deng, R. Ran, M. Liu and Z. Shao, *Adv. Energy Mater.*, 2016, **6**, 1500924.
19 T. Yuan, Z. Tan, C. Ma, J. Yang, Z. Ma and S. Zheng, *Adv. Energy Mater.*, 2017, **7**, 1601625.
20 H. Liu, Z. Zhu, J. Huang, X. He, Y. Chen, R. Zhang, R. Lin, Y. Li, S. Yu, X. Xing, Q. Yan, X. Li, M. J. Frost, K. An, J. Feng, R. Kostecki, H. Xin, S. P. Ong and P. Liu, *ACS Mater. Lett.*, 2019, **1**, 96–102.
21 M. Wagemaker, D. R. Simon, E. M. Kelder, J. Schoonman, C. Ringpfeil, U. Haake, D. Lützenkirchen-Hecht, R. Frahm and F. M. Mulder, *Adv. Mater.*, 2006, **18**, 3169–3173.
22 R. Ma, L. Shao, K. Wu, M. Shui, D. Wang, J. Pan, N. Long, Y. Ren and J. Shu, *ACS Appl. Mater. Interfaces*, 2013, **5**, 8615–8627.
23 M. Imazaki, K. Ariyoshi and T. Ohzuku, *J. Electrochem. Soc.*, 2009, **156**, A780–A786.
24 S. Wang, K. Yang, F. Gao, D. Wang and C. Shen, *RSC Adv.*, 2016, **6**, 77105–77110.
25 Z. Choi, D. Kramer and R. Mönig, *J. Power Sources*, 2013, **240**, 245–251.
26 M. Wable, B. Bal and Ö.Ö Capraz, *Energy Adv.*, 2024, **3**, 601–608.
27 H. Dykes, Rosy, D. Sharon, M. Noked and Ö. Çapraz, *J. Electrochem. Soc.*, 2021, **168**, 110551.
28 H. Dykes, S. H. Akella, B. Ozdogru, D. Sharon, M. Noked and Ö. Ö. Çapraz, *Electrochim. Acta*, 2024, **497**, 144522.
29 B. Bal, B. Ozdogru, M. Wable, V. Murugesan, G. M. Veith and Ö. Ö. Çapraz, *Electrochim. Acta*, 2024, **508**, 145223.
30 Q. V. Overmeere, J.-F. Vanhumbeeck and J. Proost, *Rev. Sci. Instrum.*, 2010, **81**, 045106.
31 D. Li and H. Zhou, *Mater. Today*, 2014, **17**, 451–463.
32 K. Mukai, T. Nonaka and T. Uyama, *Energy Storage Mater.*, 2022, **44**, 547–556.
33 B. A. Marckx, H. Maclennan and O. O. Capraz, *Chem. Biomed. Imaging*, 2025, **3**, 352–358.
34 Z. Li, B. Ozdogru, B. Bal, M. Bowden, A. Choi, Y. Zhang, H. Wang, V. Murugesan, V. G. Pol and Ö.Ö Çapraz, *Adv. Energy Mater.*, 2023, **13**, 2301329.
35 B. Bal and O. O. Çapraz, *ACS Appl. Eng. Mater.*, 2024, **2**, 2771–2776.
36 Y.-B. He, F. Ning, B. Li, Q.-S. Song, W. Lv, H. Du, D. Zhai, F. Su, Q.-H. Yang and F. Kang, *J. Power Sources*, 2012, **202**, 253–261.
37 A. Mukhopadhyay, A. Tokranov, X. Xiao and B. W. Sheldon, *Electrochim. Acta*, 2012, **66**, 28–37.
38 E. M. C. Jones, Ö.Ö Çapraz, S. R. White and N. R. Sottos, *J. Electrochem. Soc.*, 2016, **163**, A1965–A1974.
39 B. Bal, B. Ozdogru, D. T. Nguyen, Z. Li, V. Murugesan and O. O. Çapraz, *ACS Appl. Mater. Interfaces*, 2023, **15**, 42449–42459.
40 J. W. Pinder, G. H. Major, D. R. Baer, J. Terry, J. E. Whitten, J. Čechal, J. D. Crossman, A. J. Lizarbe, S. Jafari, C. D. Easton, J. Baltrusaitis, M. A. van Spronsen and M. R. Linford, *Appl. Surf. Sci. Adv.*, 2024, **19**, 100534.
41 L. Zhang, K. Zhang, Z. Shi and S. Zhang, *Langmuir*, 2017, **33**, 11164–11169.
42 M. Ma, A. N. Mansour, J. K. Ko, G. H. Waller and C. E. Hendricks, *J. Electrochem. Soc.*, 2020, **167**, 110549.
43 Y.-B. He, M. Liu, Z.-D. Huang, B. Zhang, Y. Yu, B. Li, F. Kang and J.-K. Kim, *J. Power Sources*, 2013, **239**, 269–276.
44 E. M. C. Jones, M. N. Silberstein, S. R. White and N. R. Sottos, *Exp. Mech.*, 2014, **54**, 971–985.
45 B. Özdogru, H. Dykes, D. Gregory, D. Saurel, V. Murugesan, M. Casas-Cabanas and Ö.Ö Çapraz, *J. Power Sources*, 2021, **507**, 230297.
46 Ö.Ö Çapraz, S. Rajput, K. L. Bassett, A. A. Gewirth, S. R. White and N. R. Sottos, *J. Electrochem. Soc.*, 2019, **166**, A2357–A2362.
47 L. J. Gibson and M. F. Ashby, *Cellular Solids: Structure and Properties*, Cambridge University Press, 1998.
48 J. M. Whitney and R. L. McCullough, *Micromechanical materials modeling*, Technomic Publishing Company, Inc., Lancaster, 1990.
49 X. Lu, L. Gu, Y.-S. Hu, H.-C. Chiu, H. Li, G. P. Demopoulos and L. Chen, *J. Am. Chem. Soc.*, 2015, **137**, 1581–1586.
50 Y.-B. He, B. Li, M. Liu, C. Zhang, W. Lv, C. Yang, J. Li, H. Du, B. Zhang, Q.-H. Yang, J.-K. Kim and F. Kang, *Sci. Rep.*, 2012, **2**, 913.
51 C. Han, Y.-B. He, M. Liu, B. Li, Q.-H. Yang, C.-P. Wong and F. Kang, *J. Mater. Chem. A*, 2017, **5**, 6368–6381.
52 W. Liu, H. Liu, Q. Wang, J. Zhang, B. Xia and G. Min, *J. Power Sources*, 2017, **369**, 103–110.